

Kirigami-inspired Thermal Regulator

Hongyi Ouyang,^{1,†} Yuanqing Gu,^{2,3,†} Zhibin Gao,^{1,*} Lei Hu,¹ Zhen Zhang,¹
Jie Ren,⁴ Baowen Li,⁵ Jun Sun,¹ Yan Chen,^{2,3,‡} and Xiangdong Ding^{1,§}

¹State Key Laboratory for Mechanical Behavior of Materials, Xi'an Jiaotong University, Xi'an 710049, China

²Key Laboratory of Mechanism and Equipment Design of Ministry of Education, Tianjin University, Tianjin, 300350, China

³School of Mechanical Engineering, Tianjin University, Tianjin, 300350, China

⁴Center for Phononics and Thermal Energy Science, China-EU Joint Center for Nanophonics,

Shanghai Key Laboratory of Special Artificial Microstructure Materials and Technology,

School of Physics Sciences and Engineering, Tongji University, Shanghai 200092, China

⁵Department of Materials Science and Engineering, Department of Physics, Southern University of Science and Technology, Shenzhen, 518055, PR China. International Quantum Academy, Shenzhen 518048,

PR China. Paul M. Rady Department of Mechanical Engineering and Department of Physics,

University of Colorado, Boulder, Colorado 80305-0427, USA

(Dated: February 13, 2023)

One of the current challenges in nanoscience is tailoring phononic devices such as thermal regulators and thermal computing. This has long been a rather elusive task because the thermal switching ratio is not as high as electronic analogs. Mapping from a topological kirigami assembly, nitrogen-doped porous graphene (NPG) metamaterials on the nanoscale are inversely designed with a thermal switching ratio of 27.79 which is more than double the value of previous work. We trace this behavior to the chiral folding-unfolding deformation, resulting in a metal-insulator transition. This study provides a nano-material design paradigm to bridge the gap between kinematics and functional metamaterials that motivates the development of high-performance thermal regulators.

PACS numbers: 65.80.Ck, 61.46.-w, 64.70.Nd, 71.30.+h

Thermal regulation is the most critical technology challenge for modern electronics [1, 2], thermoelectricity [3], thermal cooling [4, 5], interfacial thermal resistance [6] and phononics [7, 8]. Similar to electrical switches, thermal regulators whose thermal transport in two states or directions is relatively different from each other [9–11] and play important roles in thermal storage, thermal management and solid-state thermal circuits [12–15]. To regulate the thermal conductivity κ , researchers focused on the modulation between two states and mechanisms that facilitate large thermal switching ratio R between on-state high thermal conductivity κ_{on} and off-state low thermal conductivity κ_{off} .

Several materials have been unveiled with thermal switching behavior under different kinds of incentives [16], such as shape memory alloy [17, 18], shape-dependent nanoislands [19], monolayer lateral heterojunction [20], multi-body effect in radiation [21], strain in ferroelectric domain [22] and in compressible graphene [23], thermophile proteins [24], plasmon resonators [25], local effect in polymer [26], electric field [27, 28], magnetic field [29], temperature-induced phase transition [30], temperature-dependent transformation thermotics, element substitution [31], electrochemical reaction [32, 33], optical excitation [34] and even hydration in bio-inspired materials [35]. Although these studies have reported up to an order of magnitude in switching ratios and corresponding mechanisms, how to further augment R for high-

performance thermal regulators is still a conundrum and limits their applications.

In this Letter, we design a 2D honeycomb kirigami assembly using metamaterial and map it on porous graphene. Chirality is induced by nitrogen substitution, realizing asymmetrical folding-unfolding deformation. We find NPG can exhibit an ultrahigh R of 27.78 under only 1% strain. With this small deformation, the obvious change was found in the band structure, resulting in an unusual metal-insulator transition and enhanced optical absorption in NPG. Our work offers a nano-material design paradigm mapping from topological assembly on metamaterials, showing potential high-performance thermal regulators.

The 2D honeycomb kirigami assembly based on the nanoporous graphene with the folding-unfolding deformation, shown in Fig. 1. It consists of two modules, one of which is module I having a hexagon with 3 hinge points (light blue). Another one is module II, a similar hexagon with 6 arms (dark blue). The endpoints of the arms are connected with module I by hinges. The kirigami model enables the entire assembly with one degree-of-freedom motion and avoids physical interference. Snapshots of kirigami assembly during deformation are shown in Fig. 1(a-c), and the tessellation is presented in Fig. 1(d). The folding-unfolding deformation for the kirigami assembly is depicted in Video 1.

Geometric parameters of the kirigami assembly are illustrated in Fig. 1(e). r and d are the distance between center modules and hinge points in modules I and II, respectively. h is the distance between the center of two modules and θ is the angle between module I and the adjacent arm. A periodical rectangular unit cell was depicted in the kirigami assembly, which is more easily to determine the strain in the Cartesian

[†] These authors contributed equally to this work.

* E-mail: zhibin.gao@xjtu.edu.cn

‡ E-mail: yan_chen@tju.edu.cn

§ E-mail: dingxd@mail.xjtu.edu.cn

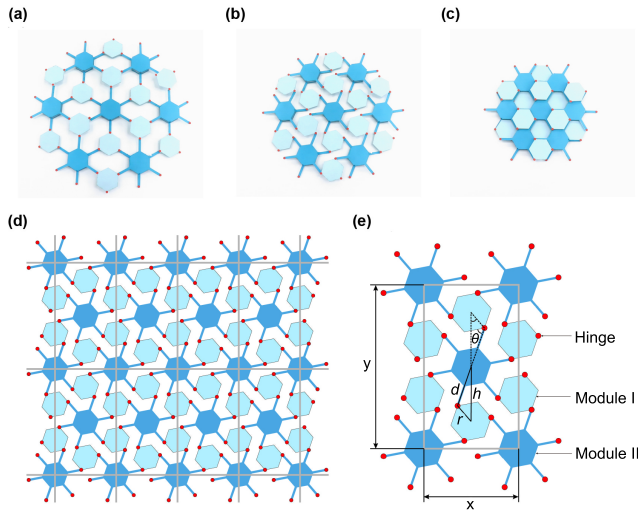


FIG. 1. Kirigami assembly consisting of regular hexagons. (a-c) Snapshots of the physical prototype in unfolding, intermediate, and fully closed states, respectively. Hinge points are shown by red dots. (d) Periodic tessellation is displayed by grey rectangles. (e) Geometric parameters are defined in the unit cell.

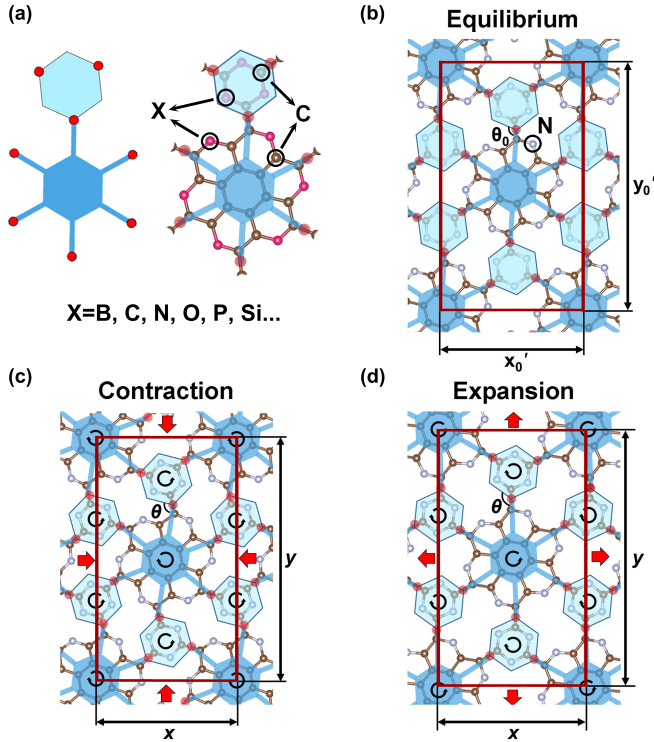


FIG. 2. Mapping of kirigami assembly to metamaterials. (a) Module I and II are replaced by one honeycomb and a cluster including seven honeycombs. The element of pink atoms labeled by X is to be decided shown in Supplemental Material. Snapshots of NPG in (b) equilibrium, (c) contraction, and (d) expansion states during deformation. Black arrows indicate the rotation of modules. The brown and white balls are C and N, respectively.

coordinate system. Then we investigate the deformation behavior of the assembly,

$$h = \sqrt{d^2 + r^2 - 2dr \cdot \cos(\theta + \pi/3)}, \quad (1)$$

$$x = \sqrt{3}h, \quad y = 3h. \quad (2)$$

In the following, we map the kirigami assembly on 2D mechanical metamaterials. The point-to-point rigid rod connections in kirigami assembly are replaced by chemical bonds. According to the spatial linkage kinematics about the relationship between cyclohexane molecular and octahedral Bricard 6R linkage [47], we call the bond connecting different modules as “hinge bond” and treat the midpoints of the “hinge bond” as hinges. Therefore, two components were designed to represent two modules in the assembly, as shown in Fig. 2(a). To increase the stability of the structure, carbocyclic six-membered rings are kept. What’s more, chirality can be induced by elemental substitution, resulting in the asymmetrical folding-unfolding deformation in metamaterials.

Since the potential element is selected, we set criteria to guide the element selection labeled X shown in Fig. 2(a), which include (i) obvious distortion out of plane should be avoided that will preclude the deformation, (ii) the connection between two types of modules should be only one chemical bond to ensure the flexibility of whole structure, (iii) the electronic band structure in the equilibrium state should be an insulator to realize the metal-insulator transition by small deformation. The whole detail of the selection process with element X is discussed in Supplemental Material [48]. Consequently, the nitrogen element is the best one of X and we focus on the nitrogen porous graphene, named NPG.

We acquired the optimized metamaterials with different lattice constants and θ by Density Function Theory (DFT). The details of calculation are shown in the Supporting Information [49–54]. Interestingly, NPG in Fig. 2(b-d) and Video 2 performs a similar folding-unfolding deformation behavior after contraction or expansion, corresponding to the kirigami assembly in Fig. 1(a-c). The most stable structure has a θ_0 of 110.73° which is slightly different from the assembly with 120° .

We unexpectedly find that NPG has a property of chirality which means the rotation in clockwise and anti-clockwise exhibit different deformation behaviors [55]. More mechanical property of NPG is discussed in the Supplemental Material.

Now we address the crucial issue, namely, deformation effect on the electronic and thermal properties. Thermal conductivity can be divided into two parts. Based on *ab initio* and non-equilibrium molecular dynamics simulation, we can obtain κ_{lat} and κ_{el} by Fourier law and Wiedemann-Franz (WF) law,

$$\kappa_{lat} = -\frac{J}{\nabla T}, \quad \kappa_{el} = L_0 \sigma T. \quad (3)$$

where J is the heat flux of energy transport per unit time across the unit area that is defined as $S = W \times d$ in which W is the width of the 2D sheet and d is the inter-layer distance for the corresponding bulk material ($d = 3.355 \text{ \AA}$ for NPG). ∇T is the temperature gradient along the heat transport direction. σ is

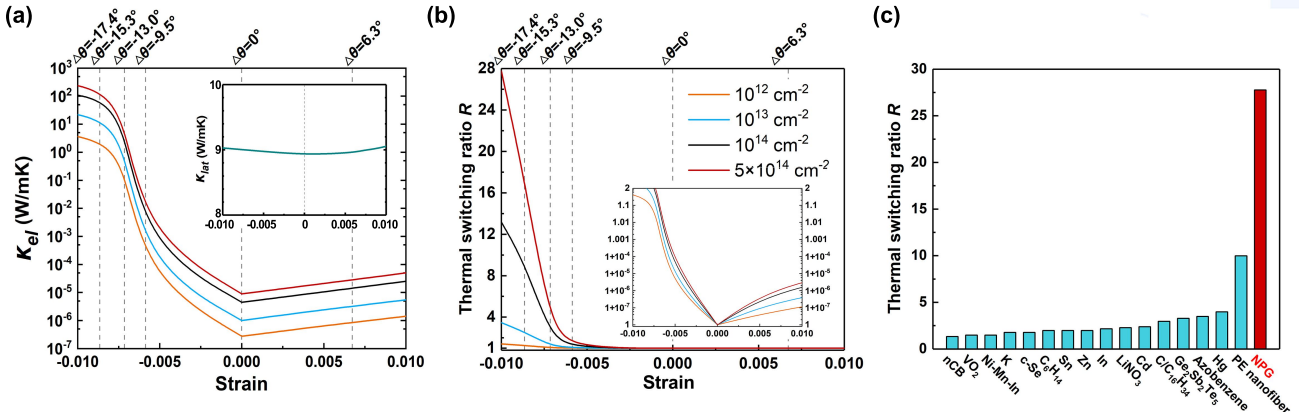


FIG. 3. (a) κ_{el} and κ_{lat} (inset) of NPG as functions of strain. (b) Thermal switching ratio R versus strain under different hole carrier concentrations. The zoom feature of R between 1 and 2 is shown in the inset. A maximum doping level of $5 \times 10^{-14} \text{ cm}^{-2}$ for both electrons and holes has been reached by electrical gating [36] and ionic liquid injection [37]. (c) R of NPG compared with reported thermal regulators. nCB [38]; VO_2 [39]; K, Zn, Cd, and Hg [40]; c-Se [41]; Ni-Mn-In alloy [42]; C_6H_{14} [43]; Sn, In, and LiNO_3 [44]; C/ $\text{C}_{16}\text{H}_{34}$ composite [45]; $\text{Ge}_2\text{Sb}_2\text{Te}_5$ [46]; azobenzene polymers [34]; PE nanofiber [30].

the electric conductivity and L_0 is the Lorenz constant number of $2.44 \times 10^{-8} \text{ W } \Omega \text{ K}^{-2}$. The discussion about why WF law is suited to NPG [56–61], details of calculation [62, 63] and length dependence of κ_{lat} [64–67] are shown in Supplemental Material.

We find that the change of κ_{lat} is not obvious as a function of strain, while κ_{el} increases by 7 orders of magnitude after contraction of only 1% strain shown in Fig. 3(a). This discovery will result in a dominating role of κ_{el} compared with κ_{lat} . κ_{lat} has a value of 8.92 W/mK in equilibrium state and fluctuates slightly to 9.05 W/mK with 1% compressive strain. κ_{el} of different doping carriers and concentrations are shown in Fig. S12.

Thermal switching ratio R is the key parameter to evaluate ability of the thermal switch, $R = \frac{\kappa_{on}}{\kappa_{off}}$, where κ_{on} is the largest κ in the “on” state, and κ_{off} is the smallest κ in the “off” state. Let us now attempt the the relationship between R and strain at four different typical doping concentrations. For instance, at $5 \times 10^{-14} \text{ cm}^{-2}$ hole doping concentration, κ_{el} is equal to $8.97 \times 10^{-6} \text{ W/mK}$ in the equilibrium state, while 238.87 W/mK with only 1% compressive strain. The total thermal conductivity changes from 8.92 W/mK without strain to 247.92 W/mK with 1% compressive strain, achieving $R = 27.79$, shown in Fig. 3(b). Furthermore, R in compressive strain is much larger than that of tensile strain, indicating an obvious chirality of NPG. At a given strain, R is directly proportional to the doping concentration, and the relative discrepancy of R between different doping levels increases as a function of strain.

Referring to most of the former research about thermal management materials such as VO_2 , PE nanofiber, and other phase change materials [30, 34, 38–46]. To the best of our knowledge, we have collected R of all these interesting works combined with our NPG value, shown in Fig. 3(c), indicating the potential of NPG for manufacturing high-performance thermal regulators.

Remember that the mild change of κ_{lat} can be originated

from the unchanged space group of NPG with $P6/m$ (175) during deformation, similar to VO_2 near the phase transition [68]. The physical reason for a wild change of κ_{el} is the metal-insulator transition, since band structures and projected density of states (PDOS) change significantly shown in Fig. 4(a–c).

With deformation, conduction bands of NPG move downward while valence bands move upward, resulting in a smaller band gap compared with the equilibrium state with $E_g = 0.73 \text{ eV}$. Under 1% compression, the band gap closes due to the decrease of distance between atoms, resulting in a shift of the electronic energy states. The projected band structure shows that the conduction band minimum is dominated by p_z orbitals of carbon and nitrogen atoms, while the valence band maximum is controlled by p_x and p_y orbitals of nitrogen atoms. Moreover, the band gap of NPG decreases slowly in expansion while declining rapidly in contraction. This phenomenon could be attributed to the chirality of NPG. We also find the main discrepancy of PDOS between the contraction state and the other two states is whether the overlap of p_x , p_y , and p_z of nitrogen atoms exists, indicating the hybridization of orbitals and delocalization of electrons.

The band gap will fall to zero when $\Delta\theta$ reaches the critical angle of -13.0° , indicating a metal-insulator transition occurs during deformation. The most adopted method to trigger it, in previous reports, is applying a large 10% mechanical deformation to adjust the distance between atoms and to redistribute electronic wavefunction, called Mott Transition [69–72]. For NPG, the metal-insulator transition emerges after only 1% change of the lattice constant, which is much easier to be realized by substrate engineering, and could be used as super-sensitive pressure sensors in nanomaterials science.

To explore electronic transport properties, we built NPG devices shown in Fig. S13. Without bias potential, transmission spectrums of different states are shown in Fig. 4(d). Around the Fermi level, there is no transmission for all of them except the state of $\Delta\theta = -13.0^\circ$ and $\Delta\theta = -17.4^\circ$, correspond-

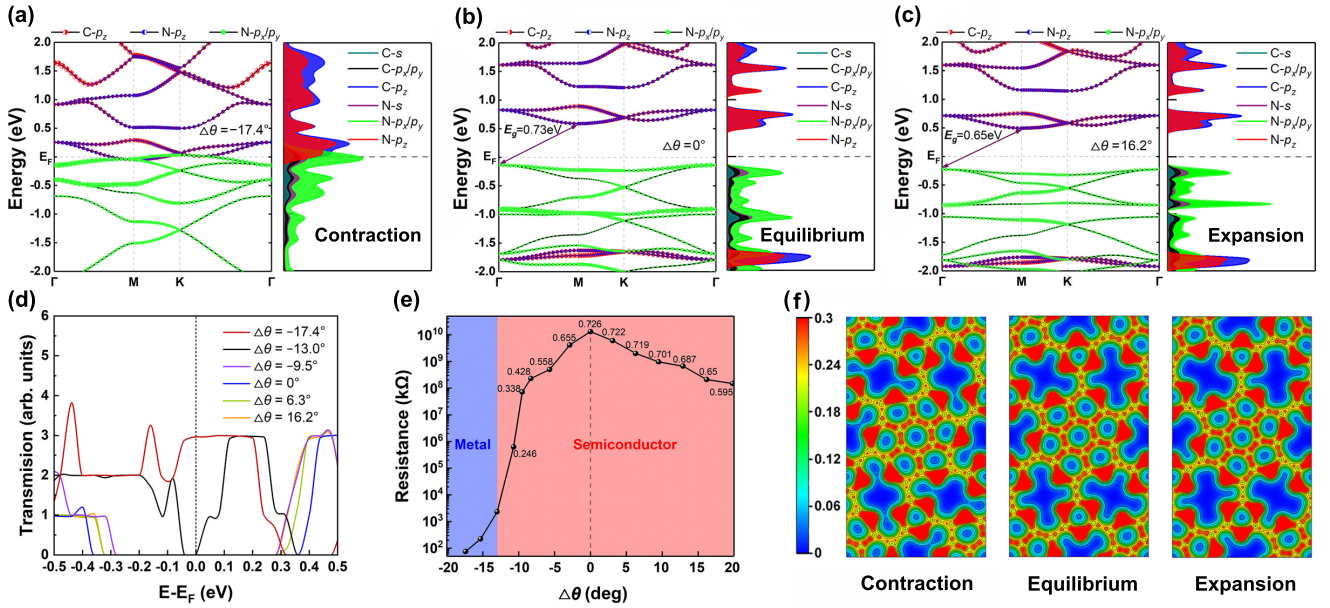


FIG. 4. (a-c) Projected band structures and PDOS of NPG in three deformation states. (d) Electronic transmission spectrum and (e) electrical resistance of NPG device with different $\Delta\theta$. Fermi level was regarded to be zero for each state to compare the transfer ability of electrons between electrodes among all states. The number in (e) stands for the band gap E_g in the eV unit. (f) The isosurface plot of the charge density of NPG and the isosurface value is taken as $0.06 e/\text{Bohr}^3$.

ing semi-metal and metal states, respectively. Then electrical resistances of different states are investigated by setting the bias voltage range from 0~1.0 V, shown in Fig. 4(e). There are 7 orders of magnitude difference in electrical resistance between the state of $\Delta\theta = -17.4^\circ$ and the equilibrium state, while only 2 orders of magnitude difference between the state of $\Delta\theta = 16.2^\circ$ and the equilibrium state. The details of calculation are shown in the Supporting Information [73–75].

Let us now attempt the mechanism of the metal-insulator transition at the electronic distribution level. Fig. 4(f) presents the charge density isosurface of NPG in three states. Contraction is more effective than an expansion to decrease the distance between adjacent nitrogen atoms, resulting in delocalizing the state and narrowing the band gap. This microscopic electronic behavior further supports the explanation of the metal-insulator transition in NPG. Except for the thermal and electrical properties, we also studied the optical property and negative thermal expansion [76, 77] of NPG shown in Fig. S16 and Fig. S17. Furthermore, we validated the effective medium concept of NPG [78] and discussed the potential methods to obtain NPG [79–87].

Before closing, we briefly discuss the energy cost to obtain such a thermal regulation. The strain energy of NPG is presented in Fig. S18, and by changing the angle θ with the $\pm 15^\circ$ from the equilibrium state, the largest energy needed is 140 meV/atom, about 3% of the carbon bond-breaking energy [88]. Thus, hexagonal rings in NPG are dynamically stable. In *ab initio* molecular dynamics calculation with two unit cells, the wrinkle along the z-axis is less than 0.05 nm in 300 K. For an extensive area of NPG, the vibration along the z-axis should be close to pure graphene, approximately equal to 1 nm [89], indicating the way of manipulating NPG is like

graphene. For instance, the strain is 0.0109 from the equilibrium state ($\theta = 110.72^\circ$) to the expansion state ($\theta = 120.27^\circ$), and the corresponding energy cost per unit cell is 3.114 eV (the area of the unit cell is 2.2458 nm²). The energy needed is 0.222 Jm⁻², even smaller than the cleavage energy of graphite with a value of 0.33 Jm⁻² [88], suggesting that NPG can be manipulated by a relatively small force.

In summary, we have exhibited the demonstration of mapping from kirigami assembly on NPG metamaterials at atomically scale whose thermal switching ratio reaches 27.79 under only 1% strain which is more than double the value of previous work. It can be stemmed from a metal-insulator transition which switches the main heat carrier in NPG during the asymmetrical folding-unfolding deformation. We hope present results for inversely designing kirigami-inspired thermal switches do invigorate the studies aimed at uncovering intriguing high-performance thermal regulators, thermal diode, and thermal transistor, in the discipline of phononics, which will play essential roles in nanoscale calorimeters and thermal management of microelectronics.

ACKNOWLEDGMENTS

We acknowledge the support from the National Natural Science Foundation of China (No. 12104356, 52071258, 52035008, 51825503) and the Tencent Foundation (XPLORER-2020-1035). Z.G. acknowledges the support of China Postdoctoral Science Foundation (No. 2022M712552) and the Fundamental Research Funds for the Central Universities. We also acknowledge the support by HPC Platform, Xi'an Jiaotong University.

- [1] M Mitchell Waldrop, The chips are down for Moore's law, *Nature* **530**, 144–147 (2016).
- [2] Philip Ball, Computer engineering: Feeling the heat, *Nature* **492**, 174–176 (2012).
- [3] Li-Dong Zhao, Shih-Han Lo, Yongsheng Zhang, Hui Sun, Gangjian Tan, Ctirad Uher, Christopher Wolverton, Vinayak P Dravid, and Mercouri G Kanatzidis, Ultralow thermal conductivity and high thermoelectric figure of merit in SnSe crystals, *Nature* **508**, 373–377 (2014).
- [4] Mengnan Jiang, Yang Wang, Fayu Liu, Hanheng Du, Yuchao Li, Huanhuan Zhang, Suet To, Steven Wang, Chin Pan, Jihong Yu, David Quéré, and Zuankai Wang, Inhibiting the Leidenfrost effect above 1,000°C for sustained thermal cooling, *Nature* **601**, 568–572 (2022).
- [5] L. Lindsay, D. A. Broido, and T. L. Reinecke, First-Principles Determination of Ultrahigh Thermal Conductivity of Boron Arsenide: A Competitor for Diamond? *Phys. Rev. Lett.* **111**, 025901 (2013).
- [6] Jie Chen, Xiangfan Xu, Jun Zhou, and Baowen Li, Interfacial thermal resistance: Past, present, and future, *Rev. Mod. Phys.* **94**, 025002 (2022).
- [7] Nianbei Li, Jie Ren, Lei Wang, Gang Zhang, Peter Hänggi, and Baowen Li, Colloquium: Phononics: Manipulating heat flow with electronic analogs and beyond, *Rev. Mod. Phys.* **84**, 1045–1066 (2012).
- [8] Xiaokun Gu, Yujie Wei, Xiaobo Yin, Baowen Li, and Ronggui Yang, Colloquium: Phononic thermal properties of two-dimensional materials, *Rev. Mod. Phys.* **90**, 041002 (2018).
- [9] Baowen Li, Lei Wang, and Giulio Casati, Thermal Diode: Rectification of Heat Flux, *Phys. Rev. Lett.* **93**, 184301 (2004).
- [10] Lei Wang and Baowen Li, Thermal Logic Gates: Computation with Phonons, *Phys. Rev. Lett.* **99**, 177208 (2007).
- [11] Chih Wei Chang, D Okawa, A Majumdar, and A Zettl, Solid-state thermal rectifier, *Science* **314**, 1121–1124 (2006).
- [12] Maria José Martínez-Pérez, Antonio Fornieri, and Francesco Giazotto, Rectification of electronic heat current by a hybrid thermal diode, *Nat. Nanotechnol.* **10**, 303–307 (2015).
- [13] Lei Wang and Baowen Li, Thermal Memory: A Storage of Phononic Information, *Phys. Rev. Lett.* **101**, 267203 (2008).
- [14] Geoff Wehmeyer, Tomohide Yabuki, Christian Monachon, Junqiao Wu, and Chris Dames, Thermal diodes, regulators, and switches: physical mechanisms and potential applications, *Appl. Phys. Rev.* **4**, 041304 (2017).
- [15] Ying Li, Wei Li, Tiancheng Han, Xu Zheng, Jiabin Li, Baowen Li, Shanhui Fan, and Cheng-Wei Qiu, Transforming heat transfer with thermal metamaterials and devices, *Nat. Rev. Mater.* **6**, 488–507 (2021).
- [16] Noé Jiménez, JP Groby, and V Romero-García, Acoustic waves in periodic structures, metamaterials, and porous media, *Ch. the Transfer Matrix Method in Acoustics*, Springer International Publishing, Cham, 103–164 (2021).
- [17] Menglong Hao, Jian Li, Saehong Park, Scott Moura, and Chris Dames, Efficient thermal management of Li-ion batteries with a passive interfacial thermal regulator based on a shape memory alloy, *Nat. Energy* **3**, 899–906 (2018).
- [18] Ying Li, Xiangying Shen, Zuhui Wu, Junying Huang, Yixuan Chen, Yushan Ni, and Jiping Huang, Temperature-dependent transformation thermotics: from switchable thermal cloaks to macroscopic thermal diodes, *Phys. Rev. Lett.* **115**, 195503 (2015).
- [19] M. Bode, O. Pietzsch, A. Kubetzka, and R. Wiesendanger, Shape-Dependent Thermal Switching Behavior of Superparamagnetic Nanoislands, *Phys. Rev. Lett.* **92**, 067201 (2004).
- [20] Yufeng Zhang, Qian Lv, Haidong Wang, Shuaiyi Zhao, Qihua Xiong, Ruitao Lv, and Xing Zhang, Simultaneous electrical and thermal rectification in a monolayer lateral heterojunction, *Science* **378**, 169–175 (2022).
- [21] Dakotah Thompson, Linxiao Zhu, Edgar Meyhofer, and Pramod Reddy, Nanoscale radiative thermal switching via multi-body effects, *Nat. Nanotechnol.* **15**, 99–104 (2020).
- [22] Eric Langenberg, Dipanjan Saha, Megan E. Holtz, Jian-Jun Wang, David Bugallo, Elias Ferreira-Vila, Hanjong Paik, Isabelle Hanke, Steffen Ganschow, David A. Muller, Long-Qing Chen, Gustau Catalan, Neus Domingo, Jonathan Malen, Darrell G. Schlom, and Francisco Rivadulla, Ferroelectric domain walls in PbTiO₃ are effective regulators of heat flow at room temperature, *Nano Lett.* **19**, 7901–7907 (2019).
- [23] Tingting Du, Zixin Xiong, Luis Delgado, Weizhi Liao, Joseph Peoples, Rajath Kantharaj, Prabudhya Roy Chowdhury, Amy Marconnet, and Xiulin Ruan, Wide range continuously tunable and fast thermal switching based on compressible graphene composite foams, *Nat. Commun.* **12**, 1–10 (2021).
- [24] Takayuki Nonoyama, Yong Woo Lee, Kumi Ota, Keigo Fujioka, Wei Hong, and Jian Ping Gong, Instant thermal switching from soft hydrogel to rigid plastics inspired by thermophile proteins, *Adv. Mater.* **32**, 1905878 (2020).
- [25] Ognjen Ilic, Nathan H Thomas, Thomas Christensen, Michelle C Sherrott, Marin Soljacic, Austin J Minnich, Owen D Miller, and Harry A Atwater, Active radiative thermal switching with graphene plasmon resonators, *ACS Nano* **12**, 2474–2481 (2018).
- [26] D. Azulay, M. Eylon, O. Eshkenazi, D. Toker, M. Balberg, N. Shimoni, O. Millo, and I. Balberg, Electrical-Thermal Switching in Carbon-Black-Polymer Composites as a Local Effect, *Phys. Rev. Lett.* **90**, 236601 (2003).
- [27] Jon F Ihlefeld, Brian M Foley, David A Scrymgeour, Joseph R Michael, Bonnie B McKenzie, Douglas L Medlin, Margeaux Wallace, Susan Trolier-McKinstry, and Patrick E Hopkins, Room-temperature voltage tunable phonon thermal conductivity via reconfigurable interfaces in ferroelectric thin films, *Nano Lett.* **15**, 1791–1795 (2015).
- [28] Chenhan Liu, Yunfei Chen, and Chris Dames, Electric-Field-Controlled Thermal Switch in Ferroelectric Materials Using First-Principles Calculations and Domain-Wall Engineering, *Phys. Rev. Applied* **11**, 044002 (2019).
- [29] Jungwoo Shin, Minjee Kang, Tsunghan Tsai, Cecilia Leal, Paul V Braun, and David G Cahill, Thermally functional liquid crystal networks by magnetic field driven molecular orientation, *ACS Macro Lett.* **5**, 955–960 (2016).
- [30] Ramesh Shrestha, Yuxuan Luan, Sunmi Shin, Teng Zhang, Xiao Luo, James S. Lundh, Wei Gong, Michael R. Bockstaller, Sukwon Choi, Tengfei Luo, Renkun Chen, Kedar Hippalgaonkar, and Sheng Shen, High-contrast and reversible polymer thermal regulator by structural phase transition, *Sci. Adv.* **5**, eaax3777 (2019).
- [31] Kiumars Aryana, Yifei Zhang, John A Tomko, Md Shafkat Bin Hoque, Eric R Hoglund, David H Olson, Joyeeta Nag, John C Read, Carlos Ríos, Juejun Hu, and Patrick E. Hopkins, Suppressed electronic contribution in thermal conductivity of Ge₂Sb₂Se₄Te, *Nat. Commun.* **12**, 1–9 (2021).
- [32] Jiung Cho, Mark D Losego, Hui Gang Zhang, Honggyu Kim, Jianmin Zuo, Ivan Petrov, David G Cahill, and Paul V Braun,

- Electrochemically tunable thermal conductivity of lithium cobalt oxide, *Nat. Commun.* **5**, 1–6 (2014).
- [33] Qiyang Lu, Samuel Huberman, Hantao Zhang, Qichen Song, Jiayue Wang, Gulin Vardar, Adrian Hunt, Iradwikanari Waluyo, Gang Chen, and Bilge Yildiz, Bi-directional tuning of thermal transport in SrCoOx with electrochemically induced phase transitions, *Nat. Mater.* **19**, 655–662 (2020).
- [34] Jungwoo Shin, Jaeuk Sung, Minjee Kang, Xu Xie, Byeongdu Lee, Kyung Min Lee, Timothy J. White, Cecilia Leal, Nancy R. Sottos, Paul V. Braun, and David G. Cahill, Light-triggered thermal conductivity switching in azobenzene polymers, *Proc. Natl Acad. Sci. USA* **116**, 5973–5978 (2019).
- [35] John A Tomko, Abdon Pena-Francesch, Huihun Jung, Madhusudan Tyagi, Benjamin D Allen, Melik C Demirel, and Patrick E Hopkins, Tunable thermal transport and reversible thermal conductivity switching in topologically networked bio-inspired materials, *Nat. Nanotechnol.* **13**, 959–964 (2018).
- [36] Dmitri K. Efetov and Philip Kim, Controlling Electron-Phonon Interactions in Graphene at Ultrahigh Carrier Densities, *Phys. Rev. Lett.* **105**, 256805 (2010).
- [37] Hsun-Jen Chuang, Xuebin Tan, Nirmal Jeevi Ghimire, Meeghage Madusanka Perera, Bhim Chamlagain, Mark Ming-Cheng Cheng, Jiaqiang Yan, David Mandrus, David Tománek, and Zhixian Zhou, High Mobility WSe₂ p- and n-Type Field-Effect Transistors Contacted by Highly Doped Graphene for Low-Resistance Contacts, *Nano Lett.* **14**, 3594–3601 (2014).
- [38] M. Marinelli, F. Mercuri, U. Zammit, and F. Scudieri, Thermal conductivity and thermal diffusivity of the cyanobiphenyl (*n*CB) homologous series, *Phys. Rev. E* **58**, 5860–5866 (1998).
- [39] Dong-Wook Oh, Changhyun Ko, Shriram Ramanathan, and David G Cahill, Thermal conductivity and dynamic heat capacity across the metal-insulator transition in thin film VO₂, *Appl. Phys. Lett.* **96**, 151906 (2010).
- [40] Cho Yen Ho, Reginald W Powell, and Peter E Liley, Thermal conductivity of the elements, *J. Phys. Chem. Ref. Data* **1**, 279–421 (1972).
- [41] GB Abdullaev, SI Mekhtieva, D Sh. Abdinov, GM Aliev, and SG Alieva, Thermal conductivity of Selenium, *Phys. Status Solidi B* **13**, 315–323 (1966).
- [42] Qiye Zheng, Gaohua Zhu, Zhu Diao, Debasish Banerjee, and David G Cahill, High contrast thermal conductivity change in Ni–Mn–In heusler alloys near room temperature, *Adv. Eng. Mater.* **21**, 1801342 (2019).
- [43] VA Konstantinov, VP Revyakin, and VV Sagan, Isochoric thermal conductivity of solid n-alkanes: hexane C₆H₁₄, *Low Temp. Phys.* **37**, 420–423 (2011).
- [44] Kwangnam Kim and Massoud Kaviani, Thermal conductivity switch: Optimal semiconductor/metal melting transition, *Phys. Rev. B* **94**, 155203 (2016).
- [45] Ruiting Zheng, Jinwei Gao, Jianjian Wang, and Gang Chen, Reversible temperature regulation of electrical and thermal conductivity using liquid–solid phase transitions, *Nat. Commun.* **2**, 289 (2011).
- [46] Luca Crespi, Andrea Ghetti, Mattia Boniardi, and Andrea L Lacaita, Electrical conductivity discontinuity at melt in phase change memory, *IEEE Electron Device Lett.* **35**, 747–749 (2014).
- [47] J Eddie Baker, Limiting positions of a Bricard linkage and their possible relevance to the cyclohexane molecule, *Mech. Mach. Theory* **21**, 253–260 (1986).
- [48] L. Tsetseris, B. Wang, and S. T. Pantelides, Substitutional doping of graphene: The role of carbon divacancies, *Phys. Rev. B* **89**, 035411 (2014).
- [49] P. E. Blöchl, Projector augmented-wave method, *Phys. Rev. B* **50**, 17953–17979 (1994).
- [50] G. Kresse and D. Joubert, From ultrasoft pseudopotentials to the projector augmented-wave method, *Phys. Rev. B* **59**, 1758–1775 (1999).
- [51] John P. Perdew, Kieron Burke, and Matthias Ernzerhof, Generalized Gradient Approximation Made Simple, *Phys. Rev. Lett.* **77**, 3865–3868 (1996).
- [52] Georg Kresse and Jürgen Furthmüller, Efficiency of ab-initio total energy calculations for metals and semiconductors using a plane-wave basis set, *Comput. Mater. Sci.* **6**, 15–50 (1996).
- [53] G. Kresse and J. Furthmüller, Efficient iterative schemes for ab initio total-energy calculations using a plane-wave basis set, *Phys. Rev. B* **54**, 11169–11186 (1996).
- [54] Hendrik J. Monkhorst and James D. Pack, Special points for Brillouin-zone integrations, *Phys. Rev. B* **13**, 5188–5192 (1976).
- [55] Corentin Coulais, Alberico Sabbadini, Fré Vink, and Martin van Hecke, Multi-step self-guided pathways for shape-changing metamaterials, *Nature* **561**, 512–515 (2018).
- [56] Jesse Crossno, Jing K Shi, Ke Wang, Xiaomeng Liu, Achim Harzheim, Andrew Lucas, Subir Sachdev, Philip Kim, Takashi Taniguchi, Kenji Watanabe, Thomas A. Ohki, and Kin Chung-fong, Observation of the Dirac fluid and the breakdown of the Wiedemann-Franz law in graphene, *Science* **351**, 1058–1061 (2016).
- [57] J Bardeen and W Shockley, Deformation potentials and mobilities in non-polar crystals, *Phys. Rev. B* **80**, 72 (1950).
- [58] Jinyang Xi, Mengqiu Long, Ling Tang, Dong Wang, and Zhigang Shuai, First-principles prediction of charge mobility in carbon and organic nanomaterials, *Nanoscale* **4**, 4348–4369 (2012).
- [59] Yongqing Cai, Gang Zhang, and Yong-Wei Zhang, Polarity-reversed robust carrier mobility in monolayer MoS₂ nanoribbons, *J. Am. Chem. Soc.* **136**, 6269–6275 (2014).
- [60] Ji-Hui Yang, Yueyu Zhang, Wan-Jian Yin, XG Gong, Boris I Yakobson, and Su-Huai Wei, Two-dimensional SiS layers with promising electronic and optoelectronic properties: theoretical prediction, *Nano Lett.* **16**, 1110–1117 (2016).
- [61] Zhili Zhu, Xiaolin Cai, Seho Yi, Jinglei Chen, Yawei Dai, Chunyao Niu, Zhengxiao Guo, Maohai Xie, Feng Liu, Jun-Hyung Cho, Yu Jia, and Zhenyu Zhang, Multivalency-driven formation of Te-based monolayer materials: a combined first-principles and experimental study, *Phys. Rev. Lett.* **119**, 106101 (2017).
- [62] Steve Plimpton, Fast parallel algorithms for short-range molecular dynamics, *J. Comput. Phys.* **117**, 1–19 (1995).
- [63] Alper Kinaci, Justin B. Haskins, Cem Sevik, and Tahir Çağın, Thermal conductivity of BN-C nanostructures, *Phys. Rev. B* **86**, 115410 (2012).
- [64] Xiangfan Xu, Luiz FC Pereira, Yu Wang, Jing Wu, Kaiwen Zhang, Xiangming Zhao, Sukang Bae, Cong Tinh Bui, Rongguo Xie, John TL Thong, Byung Hee Hong, Kian Ping Loh, Davide Donadio, Baowen Li, and Barbaros Özyilmaz, Length-dependent thermal conductivity in suspended single-layer graphene, *Nat. Commun.* **5**, 3689 (2014).
- [65] Haidong Wang, Shiqian Hu, Koji Takahashi, Xing Zhang, Hiroshi Takamatsu, and Jie Chen, Experimental study of thermal rectification in suspended monolayer graphene, *Nat. Commun.* **8**, 15843 (2017).
- [66] Stefano Lepri, Roberto Livi, and Antonio Politi, Heat Conduction in Chains of Nonlinear Oscillators, *Phys. Rev. Lett.* **78**, 1896–1899 (1997).
- [67] Zhibin Gao, Nianbei Li, and Baowen Li, Heat conduction and energy diffusion in momentum-conserving one-dimensional

- full-lattice ding-a-ling model, *Phys. Rev. E* **93**, 022102 (2016).
- [68] C. N. Berglund and H. J. Guggenheim, Electronic Properties of VO₂ near the Semiconductor-Metal Transition, *Phys. Rev.* **185**, 1022–1033 (1969).
- [69] Gerardo G Naumis, Salvador Barraza-Lopez, Maurice Oliva-Leyva, and Humberto Terrones, Electronic and optical properties of strained graphene and other strained 2D materials: a review, *Rep. Prog. Phys.* **80**, 096501 (2017).
- [70] M. Ghorbani-Asl, S. Borini, A. Kuc, and T. Heine, Strain-dependent modulation of conductivity in single-layer transition-metal dichalcogenides, *Phys. Rev. B* **87**, 235434 (2013).
- [71] Chung-Huai Chang, Xiaofeng Fan, Shi-Hsin Lin, and Jer-Lai Kuo, Orbital analysis of electronic structure and phonon dispersion in MoS₂, MoSe₂, WS₂, and WSe₂ monolayers under strain, *Phys. Rev. B* **88**, 195420 (2013).
- [72] Emilio Scalise, Michel Houssa, Geoffrey Pourtois, Valery Afanas'ev, and André Stesmans, Strain-induced semiconductor to metal transition in the two-dimensional honeycomb structure of MoS₂, *Nano Res.* **5**, 43–48 (2012).
- [73] Mads Brandbyge, José-Luis Mozos, Pablo Ordejón, Jeremy Taylor, and Kurt Stokbro, Density-functional method for nonequilibrium electron transport, *Phys. Rev. B* **65**, 165401 (2002).
- [74] Søren Smidstrup, Troels Markussen, Pieter Vancraeyveld, Jess Wellendorff, Julian Schneider, Tue Gunst, Brecht Verstichel, Daniele Stradi, Petr A Khomyakov, Ulrik G Vej-Hansen, Maeng-Eun Lee, Samuel T Chill, Filip Rasmussen, Gabriele Penazzi, Fabiano Corsetti, Ari Ojanperä, Kristian Jensen, Matthias L N Palsgaard, Umberto Martinez, Anders Blom, Mads Brandbyge, and Kurt Stokbro, QuantumATK: an integrated platform of electronic and atomic-scale modelling tools, *J. Phys.: Condens. Matter.* **32**, 015901 (2019).
- [75] Supriyo Datta, Electronic transport in mesoscopic systems, *Phys. Today* **49**, 70 (1996).
- [76] Gang Liu, Zhibin Gao, and Jie Ren, Anisotropic thermal expansion and thermodynamic properties of monolayer β -Te, *Phys. Rev. B* **99**, 195436 (2019).
- [77] Duhee Yoon, Young-Woo Son, and Hyeonsik Cheong, Negative thermal expansion coefficient of graphene measured by Raman spectroscopy, *Nano Lett.* **11**, 3227–3231 (2011).
- [78] Dan Liu, Arthur G Every, and David Tománek, Continuum approach for long-wavelength acoustic phonons in quasi-two-dimensional structures, *Phys. Rev. B* **94**, 165432 (2016).
- [79] Tetsuya Kambe, Ryota Sakamoto, Ken Hoshiko, Kenji Takada, Mariko Miyachi, Ji-Heun Ryu, Sono Sasaki, Jungeun Kim, Kazuo Nakazato, Masaki Takata, and Hiroshi Nishihara, π -Conjugated nickel bis (dithiolene) complex nanosheet, *J. Am. Chem. Soc.* **135**, 2462–2465 (2013).
- [80] Ryota Sakamoto, Kenji Takada, Tigmansu Pal, Hiroaki Maeda, Tetsuya Kambe, and Hiroshi Nishihara, Coordination nanosheets (CONASHs): strategies, structures and functions, *Chem. Commun.* **53**, 5781–5801 (2017).
- [81] Matthias Treier, Carlo Antonio Pignedoli, Teodoro Laino, Ralph Rieger, Klaus Müllen, Daniele Passerone, and Roman Fasel, Surface-assisted cyclodehydrogenation provides a synthetic route towards easily processable and chemically tailored nanographenes, *Nat. Chem.* **3**, 61–67 (2011).
- [82] César Moreno, Manuel Vilas-Varela, Bernhard Kretz, Aran Garcia-Lekue, Marius V. Costache, Markos Paradinas, Mirko Panighel, Gustavo Ceballos, Sergio O. Valenzuela, Diego Peña, and Aitor Mugarza, Bottom-up synthesis of multifunctional nanoporous graphene, *Science* **360**, 199–203 (2018).
- [83] Hiroshi Sugimoto, Minoru Fujii, and Kenji Imakita, Size-controlled growth of cubic boron phosphide nanocrystals, *RSC Adv.* **5**, 8427–8431 (2015).
- [84] Song Liu, Rui He, Lianjie Xue, Jiahan Li, Bin Liu, and James H Edgar, Single crystal growth of millimeter-sized monoisotopic hexagonal boron nitride, *Chem. Mater.* **30**, 6222–6225 (2018).
- [85] Marco Bieri, Matthias Treier, Jinming Cai, Kamel Ait-Mansour, Pascal Ruffieux, Oliver Gröning, Pierangelo Gröning, Marcel Kastler, Ralph Rieger, Xinliang Feng, Klaus Müllen, and Roman Fasel, Porous graphenes: two-dimensional polymer synthesis with atomic precision, *Chem. Commun.* **45**, 6919–6921 (2009).
- [86] Luis Francisco Villalobos, Mohammad Tohidi Vahdat, Mostapha Dakhchoune, Zahra Nadizadeh, Mounir Mensi, Emad Oveisi, Davide Campi, Nicola Marzari, and Kumar Varoon Agrawal, Large-scale synthesis of crystalline g-C₃N₄ nanosheets and high-temperature H₂ sieving from assembled films, *Sci. Adv.* **6**, eaay9851 (2020).
- [87] Qitao Tan, Huanhuan Chen, Huaida Xia, Bingxin Liu, and Bin Xu, Parent and trisubstituted triazacoronenes: synthesis, crystal structure and physicochemical properties, *Chem. Commun.* **52**, 537–540 (2016).
- [88] Wen Wang, Shuyang Dai, Xide Li, Jiarui Yang, David J Srolovitz, and Quanshui Zheng, Measurement of the cleavage energy of graphite, *Nat. Commun.* **6**, 7853 (2015).
- [89] Jannik C Meyer, Andre K Geim, Mikhail I Katsnelson, Konstantin S Novoselov, Tim J Booth, and Siegmund Roth, The structure of suspended graphene sheets, *Nature* **446**, 60–63 (2007).